frontiers in Earth Science

ORIGINAL RESEARCH
published: 12 November 2018
doi: 10.3389/feart.2018.00180

Experimental Approach to the Direct Interaction Between the H_2O-CO_2 Atmosphere and the Crust on the Earliest Earth: Implications for the Early Evolution of Minerals and the Proto-Atmosphere

Xi-Luo Hao[1,2,3] *and Yi-Liang Li*[3]*

[1] Key Laboratory of Gas Hydrate, Ministry of Natural Resources, Qingdao Institute of Marine Geology, Qingdao, China, [2] Laboratory for Marine Mineral Resources, Qingdao National Laboratory for Marine Science and Technology, Qingdao, China, [3] Department of Earth Sciences, The University of Hong Kong, Pokfulam, Hong Kong

OPEN ACCESS

Edited by:
Mónica Sánchez-Román, VU University Amsterdam, Netherlands

Reviewed by:
Nickolai Bagdassarov, Goethe-Universität Frankfurt am Main, Germany
Sujoy Ghosh, Indian Institute of Technology Kharagpur, India
Etienne Medard, Université Clermont Auvergne, France

***Correspondence:**
Yi-Liang Li
yiliang@hku.hk

Specialty section:
This article was submitted to Earth and Planetary Materials, a section of the journal Frontiers in Earth Science

Received: *15 May 2018*
Accepted: *12 October 2018*
Published: *12 November 2018*

Citation:
Hao X-L and Li Y-L (2018) Experimental Approach to the Direct Interaction Between the H_2O-CO_2 Atmosphere and the Crust on the Earliest Earth: Implications for the Early Evolution of Minerals and the Proto-Atmosphere. Front. Earth Sci. 6:180. doi: 10.3389/feart.2018.00180

Batch experiments between solid materials including komatiite, peridotite and basalt with an H_2O-CO_2 atmosphere were performed at temperatures from 200°C to 500°C to simulate the interaction between the new rocky crust formed after the magma ocean stage and the concurrent proto-atmosphere of the early Earth. Electron microscopic observations show that clay mineral flakes were generated in all experiments. In komatiite/peridotite reaction systems, fibrous actinolite was generated in experiments conducted at higher temperatures (>400°C). Different carbonate species were produced in experiments conducted at temperatures no higher than 400°C. Formation of these carbonates and their diverse crystal habits may indicate varied extraction rates of calcium, magnesium and SiO_2 from the original ultramafic rocks resulted from different experimental temperatures. Our results imply that clay minerals and carbonates could probably be formed extensively in the early Hadean by the intense interaction between the ultramafic rocky crust and the H_2O-CO_2 atmosphere before the formation of the earliest ocean. Rapid sequestration of the atmospheric CO_2 caused by the massive precipitation of carbonates might have led to the rapid cooling of the Earth's atmosphere and the formation of the earliest oceans.

Keywords: Hadean climate, phyllosilicates, carbonates, atmosphere–rock interaction, the earliest ocean

INTRODUCTION

The Hadean was the first eon that was critical for the Earth being evolved to a habitable planet and the origin of life. However, there is no petrologic record preserved for this chapter in history because of the highly active geological reworking. Right after the Moon-forming impact that occurred about 4.5 billion years ago (Valley et al., 2014), the surface of the Earth probably turned into a magma ocean and was too hot for life to start. Therefore, there should be some critical steps for the early Earth to evolve from a fiery hell to a habitable planet in the Hadean. The direct interaction between the proto-atmosphere and the newly solidified crust was probably one of these important steps

because of its impact on the chemistries of the early atmosphere, the very surface of the crust and latterly, the formation of the ocean.

Since the geological record of the Hadean eon have been destroyed by the highly active plate tectonics, mountain building and erosion (Martin et al., 2006), the primordial mineralogical composition of the Earth's surface is still a mystery. Constrained by the evolution of the magma ocean, the earliest Earth's surface (newly solidified proto-crust) was speculated to be basaltic/komatiitic in composition (Martin et al., 2006). The composition of the Earth's earliest atmosphere is also debatable. Assuming that it was produced during the late planetary accretion by early magmatic degassing processes (Shaw, 2008), including impact degassing (e.g., Lange and Ahrens, 1982; Ahrens et al., 1989) and volcanic degassing (e.g., Holland, 1984), the detailed degassing processes are critical in determining the species of the produced gasses. For instance, the gas species produced before and after the sinking of Fe–Ni into the core might have different oxidation states (Holland, 1984). Previous studies of the trace elements of mantle-derived komatiites, kimberlites, basalts, volcanic materials and zircons suggested that the oxidation state of the uppermost mantle was within ±2 log units of the fayalite-magnetite-quartz (FMQ) buffer probably at ∼4.4 billion years ago (Canil, 1997; Delano, 2001; Li and Lee, 2004; Trail et al., 2011). In equilibrium with this relatively oxidized mantle, magmatic degassing would have probably generated gasses mainly composed of CO_2 and H_2O (Trail et al., 2011). Assuming that this magmatic degassing process dominated at this stage, the early atmosphere of the Earth would mainly consist of CO_2 and H_2O around 4.4 Ga when the earliest ocean formed. Several studies have suggested that the early atmosphere of the Earth was likely composed of several tens MPa of water steam, 4–21 MPa of CO_2 and small amount of CO, H_2, etc. (Condie, 1980; Walker, 1985; Liu, 2004; Zahnle, 2006; Zahnle et al., 2007; Sleep, 2010) a few million years after the Moon-forming impact. The continuous cooling of the Earth's surface led to the condensation of the atmospheric water steam, and subsequently, the formation of the earliest ocean before 4.4 Ga (Wilde et al., 2001; Pinti, 2005; Martin et al., 2006; Valley et al., 2014). Since the proto-atmosphere was probably enriched in CO_2 (Kasting, 1993; Sleep and Zahnle, 2001), clay minerals and carbonates could be produced by fluid-rock interactions at an early age (Hazen et al., 2013). However, no outcrops with an unambiguous age older than 4.3 billion years could survive the dynamic evolution of the Earth (Tessalina et al., 2010). Thus, the existence of clay minerals and ancient carbonates on the Hadean Earth is speculative and void of solid supporting evidence.

Experiments (Berndt et al., 1996; Seyfried et al., 2007; Marcaillou et al., 2011) with similar P-T conditions to the earliest Earth have been conducted to study the process of serpentinization in the presence of liquid water. However, the reactions in these experiments could be quite different from a direct interactions between the H_2O-CO_2 atmosphere and ultramafic rocks, since CO_2 was either not included or added as a minor component in the form of sodium bicarbonate in studies on the abiotic synthesis of hydrocarbons (Berndt et al., 1996; Seyfried et al., 2007; Marcaillou et al., 2011). Moreover, most of the experimental data were acquired at temperatures on or below 300°C. In recent years, the reaction between ultramafic/mafic rocks and minerals and CO_2-rich fluid has gained more interest and several experiments have been conducted to study the carbonation process in the reaction (Dufaud et al., 2009; Jones et al., 2010; Klein and McCollom, 2013; Shibuya et al., 2013). These studies suggested that the existence of high levels of CO_2 could significantly change the resulting minerals and affect the generation of CH_4 by the formation of carbonates. Although certain amounts of CO_2 were added in these experiments, its applied concentrations were not high enough for the reaction to represent the interaction between the H_2O-CO_2 atmosphere and ultramafic rocks before the formation of the ocean. Therefore, the mineralogical consequence of this direct interaction and the generation of hydrogen and hydrocarbons during this process need reassessment. Recently, the model of the mineral evolution on the Hadean Earth proposed by Hazen et al. (2008, 2013) suggested that the interactions between Earth's atmosphere, lithosphere and hydrosphere would lead to a widespread serpentinization of Earth's mafic crust and result in the first significant production of clay minerals, with magnesite as a possible accessory mineral. Hazen's models did not consider the direct interaction between the H_2O-CO_2 proto-atmosphere and proto-crust before the formation of the earliest ocean. This process happened prior to the aqueous alteration of the proto-crust and its impact on the mineralogical diversification has not yet been experimentally tested.

In this study, experiments were carried out to simulate the direct interaction between the rocky crust and the proto-atmosphere of the early Hadean Earth. By examination of the formation of secondary minerals, hydrogen and hydrocarbons, we suggest the mineral evolution coupled the thermal and chemical evolutions of the atmosphere and ocean that have led to the formation of a habitable environment on the Earth at a very early age.

MATERIALS AND METHODS

As the reduced chemical species (i.e., CO, CH_4, and H_2) in the proto-atmosphere only constituted small fractions of Earth's earliest atmosphere (Condie, 1980; Walker, 1985; Liu, 2004; Zahnle, 2006; Zahnle et al., 2007; Sleep, 2010), they probably would not play substantial roles in the interaction between the proto-atmosphere and the ultramafic crust. Therefore, a H_2O-CO_2 system was used to represent the main geochemically active compositions of the proto-atmosphere. In our experiments, we used the following materials to represent the earliest crustal ultramafic/mafic rocks: fresh komatiite from Zimbabwe with a high Mg content and a relatively high content of Ni and Cr (Nisbet et al., 1987; Berry et al., 2008), peridotite xenolith hosted by alkali basalts from the Panshishan of Jiangsu Province of eastern China (Yu et al., 2005a,b; Hao and Li, 2013), and iron-rich alkali basalt from the Dahalajunshan Formation in the northeast Ili Block of western Tianshan. The mineralogy and chemical compositions of the starting rocks are summarized in the **Supplementary Table S1**. The values of $Fe^{2+}/\Sigma Fe$ in komatiite

and basalt were measured by ^{57}Fe Mössbauer spectroscopy (MS) with a 25mCi ^{57}Co/Pb source at the University of Hong Kong. For MS measurements, the finely ground rock samples were mounted in an acrylic holder with relative thicknesses of ∼5 mg Fe/cm^2. Spectra were collected at room temperature in transmission mode with a constant acceleration mode. The velocity scale was calibrated relative to a 25-μm α-Fe foil at room temperature. Lorentzian doublets were used for fitting the areas of the paramagnetic doublets in those silicates.

The experiments were carried out at the Hydrothermal Laboratory at Guangzhou Institute of Geochemistry, Chinese Academy of Sciences. Fresh $Ag_2C_2O_4$, distilled deionized water and powdered rock samples (<200 mesh) were weighed and loaded into a flexible Au capsule, which was subsequently sealed by a welding machine in an atmosphere of argon. The water-rock ratio (weight ratio) was adjusted to approximately 2:1, and $Ag_2C_2O_4$ was restricted to a suitable amount to avoid the explosion of the sealed Au capsule. The sealed Au capsule was then put into a steel alloy autoclave. The pressure inside the autoclave was maintained by the injection of argon gas using a booster pump and was monitored by a barometer. A digital temperature controller was used to maintain a constant temperature. Batch experiments were carried out by heating the autoclave to a constant temperature under 50 MPa pressure for 2 weeks. For the komatiite-(H_2O-CO_2) system, the temperature of batch experiments varied from 200 to 500°C with an increment of 50°C; while for the peridotite/basalt-(H_2O-CO_2) systems, the temperature of batch experiments varied from 200 to 500°C with an increment of 100°C. At the end of each experiment, the autoclave was quenched to room temperature quickly with ice water. Experiments loaded with a small piece of komatiite (∼4 mm), $Ag_2C_2O_4$ and H_2O were also conducted to study the contact feature of the secondary minerals and the precursor rock. Control experiments loaded with rock samples, pure $Ag_2C_2O_4$ and water were performed at varied temperatures (see **Supplementary Table S2**) to examine the possible gas products of thermal decomposition of rock samples or $Ag_2C_2O_4$. The experimental conditions are summarized in **Table 1**.

The solid products of batch experiments were investigated by a Hitachi S-4800 field emission scanning electron microscope (SEM) and a LEO 1530 FEG SEM at the University of Hong Kong. Each sample was distributed on a small piece of silica plate by ethyl alcohol. The sample was then coated with an ultra-thin film of Au before being placed in the sample chamber of SEM. For SEM observation, the accelerating voltage was set to 3–5 kV to capture the secondary electron images, typically showing detailed surface morphology. Energy dispersive X-ray spectroscopy (EDS) measurement was also carried out at 20 kV to measure the *in situ* chemical compositions. The EDS analyses could only provide limited information because the secondary minerals often adhered to the host rock and contributed strong background signals. A FEI Tecnai G2 20 S-TWIN Scanning Transmission Electron Microscope (STEM) was used to characterize the crystallographic structures of the secondary minerals. Specimens were loaded on copper grids with carbon-coated formvar and examined in the normal STEM mode to obtain bright images using an accelerating voltage of 200 kV. Detailed structural information of minerals was obtained by selected area electron diffraction (SAED) patterns and high-resolution transmission electron microscopy (HRTEM) micrographs.

At the end of each experiment, the volatile components in the Au capsule were analyzed by an Agilent 6890N gas chromatograph (GC) connected with a gas-collection system at Guangzhou Institute of Geochemistry, Chinese Academy of Sciences. Firstly, the sealed Au capsule was cleaned and put into the gas-collection system. After the whole system was evacuated, the Au capsule was pierced and the sealed volatile components would fill the gas-collection system. Then the valve between the gas-collection system and the 6890N GC was opened to allow gasses to diffuse into the GC. The schematic diagram of the gas-collection system is shown in **Figure 1**. The concentration of H_2 and hydrocarbons sealed in the Au capsule were analyzed in an automatically controlled procedure. The analytical results are summarized in **Table 2**.

RESULTS

Mössbauer Spectroscopy and $Fe^{2+}/\Sigma Fe$ of the Rock Samples

The komatiite and basalt used in these experiments consist of multiple minerals/materials that showed multiple crystallographic sites of Fe^{2+} and Fe^{3+}. As a result, the MS profile of komatiite was fitted with two Fe^{2+}-doublets and one Fe^{3+}-doublet (**Figure 2**). The doublet with QS = 0.53 mm/s and IS = 0.25 mm/s was assigned to paramagnetic Fe^{3+} in silicates; while the doublet with QS = 2.58 mm/s and IS = 1.01 mm/s and the doublet with QS = 1.85 mm/s and IS = 1.02 mm/s were both assigned to paramagnetic Fe^{2+} in silicates. The $Fe^{2+}/\Sigma Fe$ value of the initial komatiite was 0.91 based on the fitting of the spectrum. Similarly, the spectroscopic profile of basalt was also fitted with two Fe^{2+}-doublets and one Fe^{3+}-doublet (**Figure 2**). As the result of MS of basalt, the doublet with QS = 0.46 mm/s and IS = 0.22 mm/s was assigned to paramagnetic Fe^{3+} in silicates; while the doublet with QS = 2.53 mm/s and IS = 1.01 mm/s and the doublet with QS = 2.17 mm/s and IS = 0.96 mm/s were both assigned to paramagnetic Fe^{2+} in silicates. The $Fe^{2+}/\Sigma Fe$ value of the basalt was 0.67 based on the fitting of the spectrum. The MS and $Fe^{2+}/\Sigma Fe$ values of the minerals in peridotite have been reported previously ($Fe^{3+}/\Sigma Fe_{ol}$ = 0, $Fe^{3+}/\Sigma Fe_{opx}$ = 0.08–0.13, $Fe^{3+}/\Sigma Fe_{cpx}$ = 0.19–0.31, $Fe^{3+}/\Sigma Fe_{sp}$ = 0.13–0.23) (Hao and Li, 2013). The relatively high $Fe^{2+}/\Sigma Fe$ values for these ultramafic/mafic rocks indicate that they undergo negligible alteration and are suitable for the batch experiments.

Crystallography of Clay Minerals

Komatiite-H_2O-CO_2 System

Clay minerals, of various sizes and flaky structures, were the most abundant secondary minerals that could be observed in the komatiite-(H_2O-CO_2) experiments carried out from 200 to 500°C (**Figure 3**). The EDS analysis showed that the subsequently formed clay minerals contained substantial amounts of Si (20.0 wt%), Al (2.9 wt%), Mg (15.0 wt%), and Fe (5.9 wt%). The

TABLE 1 | Summary of the initial experimental conditions of batch experiments.

Experiment #	Initial materials			Calculated initial CO_2/H_2O (mol/mol)	Temperature (°C)	Pressure (MPa)	Run duration (days)
	Rock powder (mg)	$Ag_2C_2O_4$ (mg)	H_2O (mg)				
	Komatiite-[H_2O-CO_2] steam system						
K-500P[a]	31.6	22.7	64.1	0.0419	500	50	14
K-500M[b]	NA	22.6	60.3	0.0444	500	50	14
K-450P	35.2	26.7	68.8	0.0460	450	50	14
K-450M	NA	25.4	70.1	0.0429	450	50	14
K-400P	32.1	23.1	61.7	0.0443	400	50	14
K-400M	NA	27.4	60.4	0.0537	400	50	14
K-350P	26.4	26.9	51.3	0.0621	350	50	14
K-300P	27.6	25.2	50.1	0.0596	300	50	14
K-250P	23.8	26.4	52.4	0.0597	250	50	14
K-200P	24.1	24.7	50.9	0.0575	200	50	14
	Basalt-[H_2O-CO_2] steam system						
B-500P	33.6	23.2	64.9	0.0423	500	50	14
B-400P	34.1	24.1	68.2	0.0418	400	50	14
B-300P	35.6	26.4	70.1	0.0446	300	50	14
B-200P	30.1	24.8	61.8	0.0475	200	50	14
	Peridotite-[H_2O-CO_2] steam system						
P-500P	33.9	21.9	69.3	0.0374	500	50	14
P-400P	36.1	23.7	69.9	0.0402	400	50	14
P-300P	33.0	25.0	66.3	0.0447	300	50	14
P-200P	31.1	26.1	65.7	0.0470	200	50	14

[a] *Powdered rock sample (200 mesh).* [b] *Small piece of sample (diameter ∼4 mm).*

SEM and TEM images showed that the clay minerals generally occurred as irregularly-shaped thin flat sheets with the thickness of a few tens of nm, although some crystals have subhedral or euhedral outlines displaying 60 or 120° angles. SAED analysis of the clay crystals yielding (hkl) of (110), (200), (040), (310), and (330), indicating the electron diffraction pattern of the disordered stacking of individual crystals of Mg–Fe–Al smectite (**Figure 3F**). The formation of smectite was also indicated by the presence of a sharp hexagonal lattice embedded in the ring (**Figure 3F**).

Peridotite-H_2O-CO_2 System

Clay minerals were also identified in peridotite-(H_2O-CO_2) experiments conducted from 200 to 500°C (**Figure 4**). SEM observations showed flaky structures similar to the clay mineral found in the komatiite-(H_2O-CO_2) system (**Figure 3**). EDS results showed that the clay minerals contained mainly Mg and Fe besides Si and O. SAED analysis of the clay crystals formed at the temperatures of 400 and 500°C (**Figures 4G,H,J,K**) yielded similar diffraction pattern as Mg–Fe–Al smectite. However, the clay minerals formed in lower temperature experiments (200 and 300°C) did not generate diffraction rings in SAED patterns but had similar chemical compositions, indicating their amorphous nature (**Figures 4I,L**). The different crystallinities of the Mg–Fe smectite in the experiments imply that the higher temperatures favor better crystallinity.

Basalt-H_2O-CO_2 System

Clay minerals were also identified in basalt-(H_2O-CO_2) experiments conducted from 200 to 500°C (**Figure 5**). Different from the above two reaction systems, the clay minerals formed in the basalt-(H_2O-CO_2) system appeared as more regular hexagonal tablets with the size of a few μm and the thickness of ∼100 nm at higher temperatures (400 and 500°C). EDS analysis showed that the clay mineral contains substantial amounts of K (∼5.2 wt%) besides Mg, Fe, Al, Si, and O. SAED analysis of crystals generated a set of clear diffraction spots. Together with the EDS measured chemical composition, this clay mineral was confirmed to be illite.

Crystallography of Carbonates

Calcium Carbonate

Calcium carbonate was identified in the komatiite-(H_2O-CO_2) experiments carried out at 400°C and basalt-(H_2O-CO_2) experiments conducted at 300°C (**Figure 6**). The SEM observation showed that the calcium carbonate formed in both reaction systems were rhombohedral polycrystals of a few μm in size. EDS analysis showed that the mineral

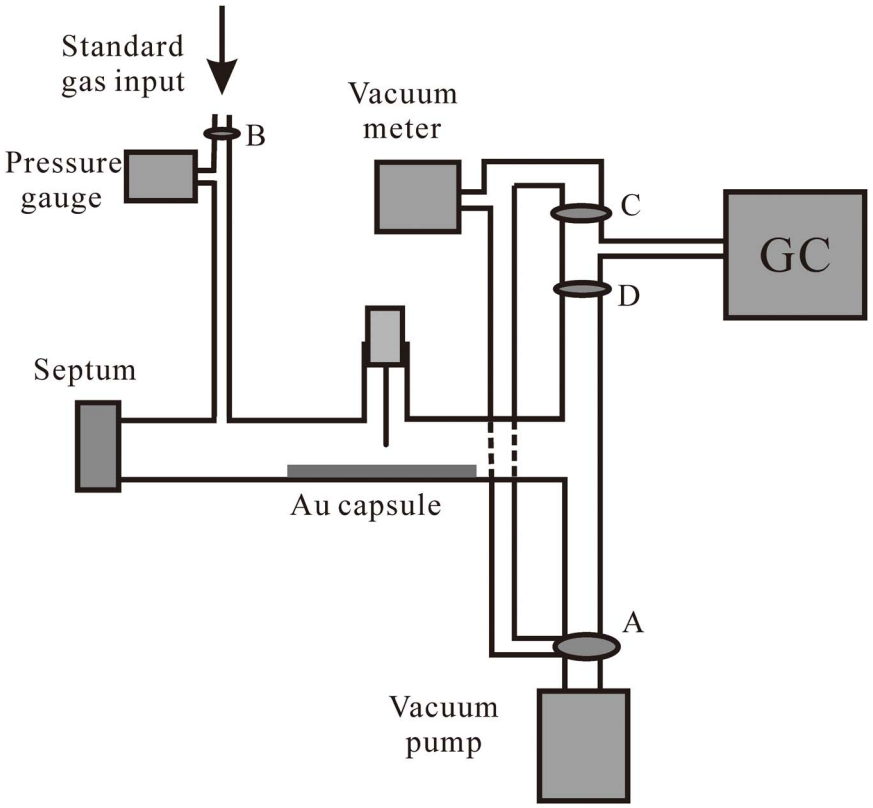

FIGURE 1 | Schematic diagram of the gas collection system connected with GC. After the sealed Au capsule was cleaned and put into the gas-collection system. Valve B was closed while valves A, C, and D were open. The whole system was evacuated by the vacuum pump. Then the Au capsule was pierced by the needle on top of it to release the sealed volatile components which would then fill the space entrapped by valves A, B, and D. Finally, valve D was open to allow the gasses to be analyzed by the 6890N GC.

TABLE 2 | GC measurements of hydrogen and light alkanes produced in the batch experiments.

	Komatiite-H_2O-CO_2							Peridotite-H_2O-CO_2				Basalt-H_2O-CO_2			
Temperature (°C)	**200**	**250**	**300**	**350**	**400**	**450**	**500**	**200**	**300**	**400**	**500**	**200**	**300**	**400**	**500**
Vol% in Au capsule															
CH_4	0.002	0.05	0.08	0.03	0.10	0.13	0.26	0.00	0.21	0.13	0.37	0.001	0.003	0.02	0.57
C_2H_6	0.00	0.01	0.01	0.01	0.01	0.02	0.07	0.00	0.003	0.02	0.04	0.00	0.00	0.002	0.14
C_3H_8	0.001	0.02	0.01	0.01	0.01	0.003	0.00	0.00	0.003	0.02	0.00	0.00	0.00	0.001	0.00
H_2	0.01	0.04	0.06	0.02	0.20	0.13	0.13	0.02	0.14	0.03	0.07	0.002	0.02	0.008	0.07
CO_2	97.5	97.2	96.5	97.3	97.3	98.7	98.1	96.1	96.5	97.2	97.1	97.6	97.0	97.8	96.8
N_2*	2.51	2.68	3.34	2.72	2.39	1.19	1.43	3.85	3.17	2.62	2.38	2.37	3.04	2.16	2.49

N_2 came from the carrier gas during the analyses.

contained small amounts of Mg (∼1.9 wt%) and Fe (∼0.6 wt%). The obtained SAED pattern showed clear diffraction spots, indicating the high crystallinity of calcite. Experiments loaded with a small piece of komatiite (∼4 mm in diameter) showed that calcite crystals mainly stacked on the glass matrix (**Figure 7**), which is the Ca-containing part of komatiite (5.0 wt% Mg, 5.0 wt% Al, 16.1 wt% Ca, and 12.6 wt% Fe as measured by EDS). This close relationship indicated the extraction of Ca from the glass matrix under the experimental conditions.

Magnesium Carbonate

In komatiite-(H_2O-CO_2) experiments, magnesium carbonate was generated at 200 and 250°C (**Figure 8**). Similar to calcite, magnesite crystals (MCs) also appeared as rhombohedral polycrystals of a few μm in size. In the peridotite-(H_2O-CO_2) system, MCs were observed in experiments carried out at 200 and 300°C. In the 300°C experiment, magnesite showed a similar crystal shape as that in the komatiite-(H_2O-CO_2) experiments; while in the 200°C experiment, MCs appeared as dodecahedron polycrystals with a uniform size of 2–3 μm (**Figure 9**).

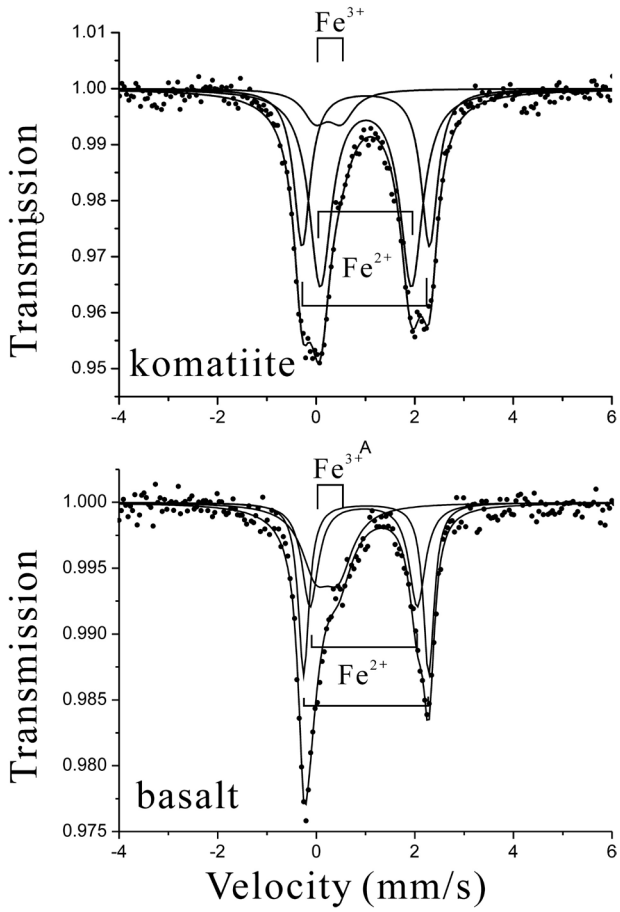

FIGURE 2 | Mössbauer spectroscopy of komatiite and basalt used for the batch experiments. As both komatiite and basalt are made of multiple minerals/materials with multiple crystallographic sites of Fe^{2+} and Fe^{3+}, their Mössbauer spectroscopic profiles were fitted with two paramagnetic Fe^{2+}-doublets and one Fe^{3+}-doublet.

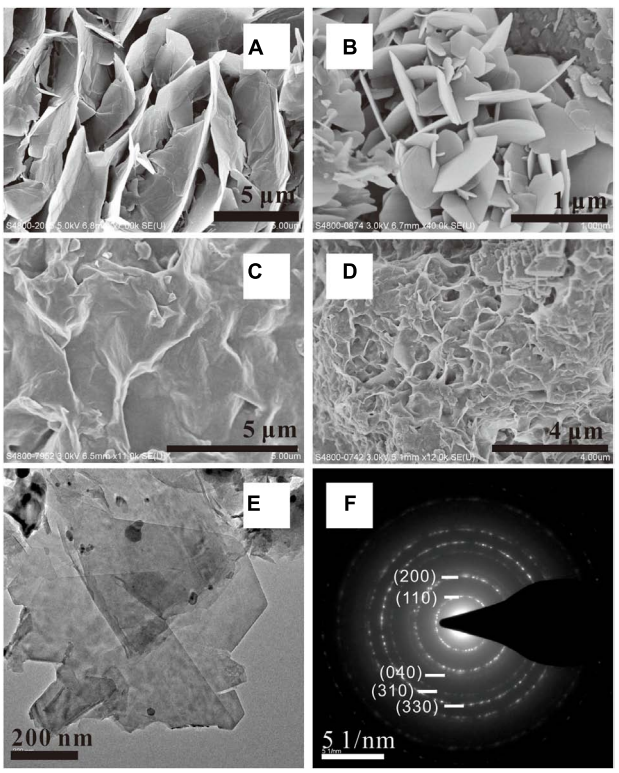

FIGURE 3 | SEM **(A–D)** and TEM **(E)** observations of Mg–Al–Fe smectite formed in [H_2O-CO_2]-komatiite system. The SAED pattern **(F)** shows clear diffraction rings indicating disordered stacking of individual crystal.

Ca–Mg Carbonates

In three reaction systems, Ca–Mg carbonates formed at different temperatures. It formed at 300–350°C, 400°C, and 200°C in the komatiite-(H_2O-CO_2) system, peridotite-(H_2O-CO_2) system and basalt-(H_2O-CO_2) system, respectively. Similar to calcite crystals, the crystals formed in all systems appeared as rhombohedrons (**Figure 10**) and were determined by SAED to be dolomite in structure. Surface morphologies of dolomite crystals in komatiite-(H_2O-CO_2) system changed along with the starting states of the initial komatiite. Smooth polyhedral single-crystal particles were formed from small pieces of komatiite (∼4 mm) (**Figure 10A**) while crystallite aggregations with rough surfaces were obtained from the powdered komatiite (**Figure 10C**).

Crystallography of the Other Silicates

Silicates other than clay minerals and carbonates were also identified in komatiite-(H_2O-CO_2) and peridotite-(H_2O-CO_2) systems with experimental temperatures higher than 450°C. SEM and TEM observations showed that the silicate crystals occurred as fibrous bundles that could grow up to a few tens of μm long (**Figure 11**). EDS analysis indicated that the silicate was mainly composed of Si, O, Ca, Mg, Fe, and trace Al. The SAED pattern of the crystals showed a set of clear diffraction spots (**Figure 11F**). Combined with its chemical compositions, the silicate was determined to be actinolite. HRTEM images of crystals showed clear lattice fringes, indicating their monocrystalline nature. The measured spacing values of the crystallographic planes were 0.845, 0.509, and 0.452 nm (**Figure 11E**) for the monocrystal, which were close to the d-spacing of (110), (001), and (040) planes of actinolite crystals.

Hydrogen and Hydrocarbons Produced in the Batch Experiments

Hydrogen was produced in all the three reaction systems at all experimental temperatures (from 200 to 500°C). When experimental temperatures were lower than 400°C, the productivity rate of H_2 was relatively low and showed no obvious correlation with temperature, especially for peridotite/basalt reaction systems. The generation of H_2 was enhanced when the experiments were conducted at 500°C. CH_4 was produced in most experiments, except the one conducted at 200°C for the peridotite-(H_2O-CO_2) reaction system. Higher temperatures would lead to higher productivity rates of CH_4. The productions

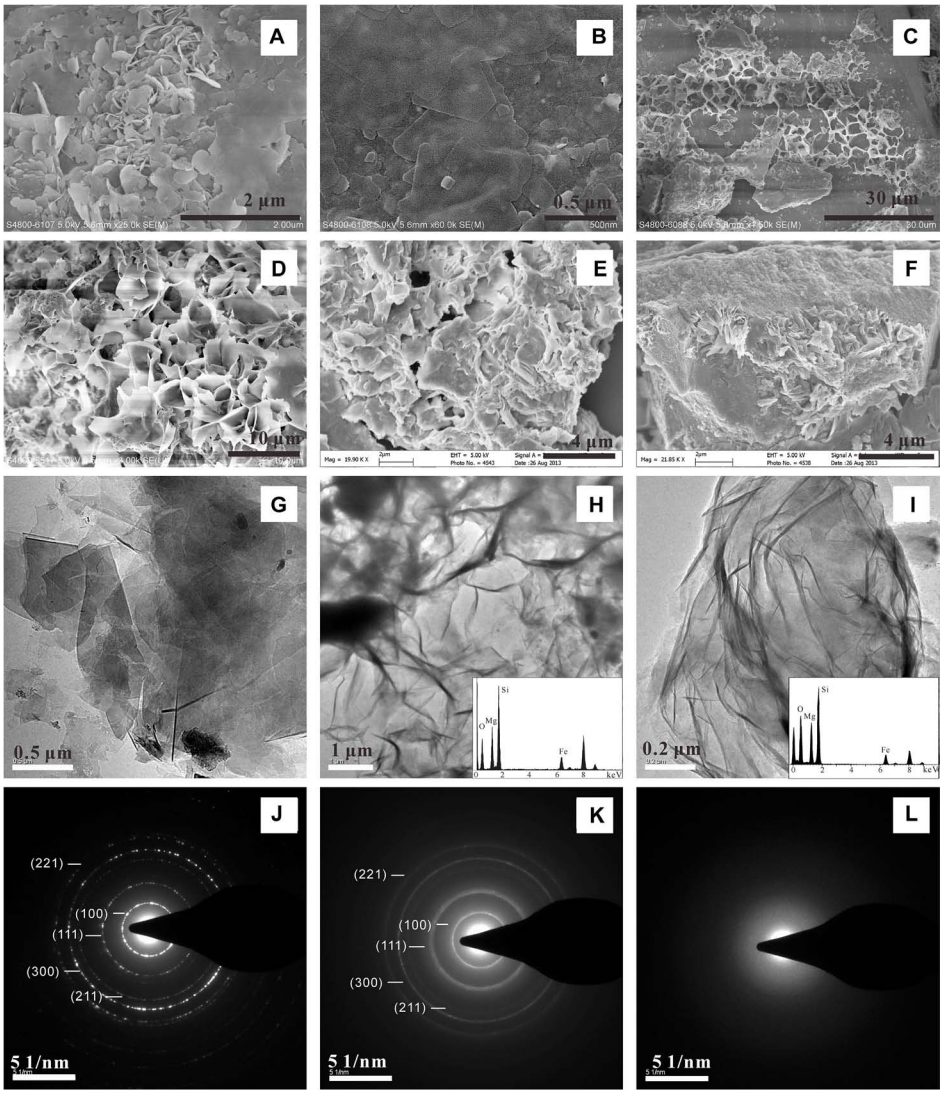

FIGURE 4 | SEM **(A–F)** and TEM **(G–I)** characterizations of Mg–Fe smectite produced in [H_2O-CO_2]-peridotite system. The SAED patterns show well crystallized **(J,K)** Mg–Fe smectite and amorphous **(L)** Mg–Fe smectite formed in high and low temperature experiments, respectively.

of C_2H_6 and C_3H_8 were GC-detectable in the three reaction systems at relatively higher temperatures, which were much lower than that of the CH_4 in the same experiment (**Table 2**).

DISCUSSION

Experimental Conditions Constrained Clay and Carbonate Speciation

Clay Speciation

Clay minerals can be observed in all experiments at various temperatures. The results show straightforward evidence that the speciation of clay minerals was only affected by the petrologic features of the precursor ultramafic/mafic rocks. The change of experimental temperature appears to contribute to the nature of the crystallinity but has little influence on the chemical composition. In the komatiite- and peridotite-systems, the formed clay minerals appear similar and they both belong to the smectite group. The difference between these two kinds of clay minerals is the concentration of Al. Possibly owing to the different Al-containing materials in komatiite and peridotite, smectite formed in komatiite-(H_2O-CO_2) systems contains substantial amounts of Al, which is, however, negligible in smectite formed in peridotite-(H_2O-CO_2) systems. For komatiite system, the main Al-containing part is the glass matrix that is much easier to be altered than that in peridotite (spinel and pyroxenes). Therefore, the alteration of komatiite is likely to result in relatively higher activity of Al in the fluid and lead to the partitioning of Al into smectite. The alteration of alkali basalt has subtle difference from that of komatiite and peridotite. Due likely to its substantial amount of K (2.96 wt% K_2O by EPMA), the activity of alkali metal ions (e.g. K^+) could be higher in the fluid

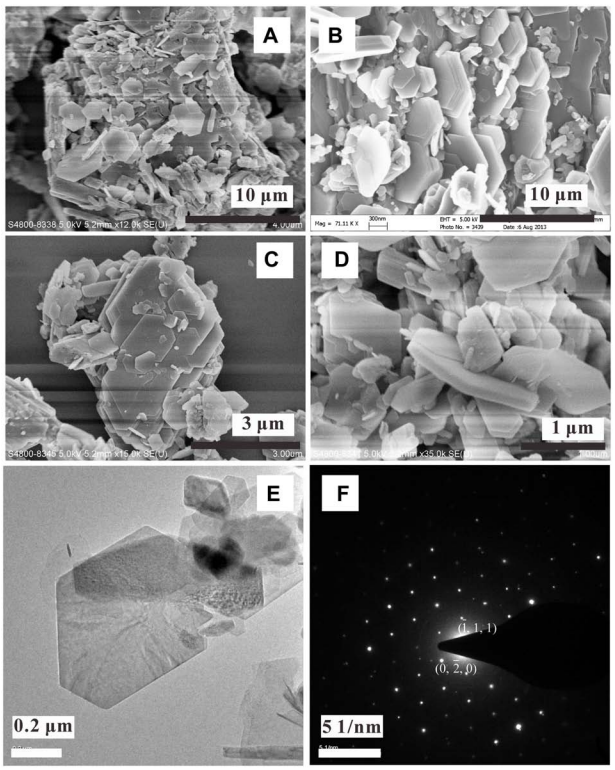

FIGURE 5 | SEM **(A–D)** and TEM **(E)** characterizations of illite formed in [H_2O-CO_2]-basalt system. The SAED pattern **(F)** shows a set of clear diffraction spots indicating single crystalline nature.

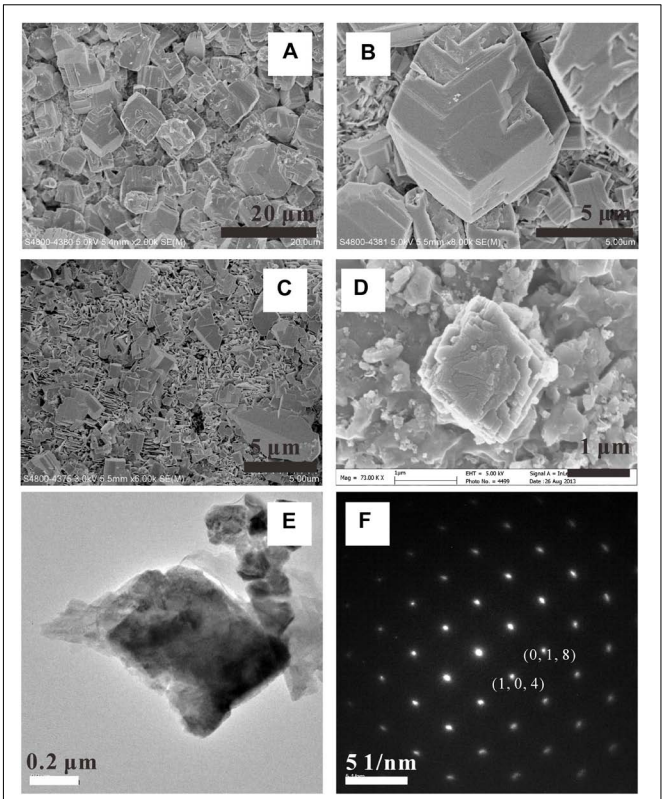

FIGURE 6 | SEM observations of calcite crystals formed in the [H_2O-CO_2]-komatiite system **(A–C)** and [H_2O-CO_2]-basalt system **(D)**. **(F)** TEM image of calcite and the related SAED pattern **(E)**.

and lead to the formation of illite rather than smectite. It is worth noting that the alkali basalt contains almost 10 times more K_2O than the tholeiitic basalt (Pearce, 1976). Using regular tholeiitic basalt as the starting material in the basalt reaction system would decrease the activity of K^+ in the solution. In this case, the run products would be no difference in the three reaction systems in terms of clay minerals.

Since the experimental P-T conditions of previous experiments in H_2O-system (Berndt et al., 1996; Seyfried et al., 2007) are similar to those in this study, serpentine, as an important secondary minerals commonly found in these studies, was never observed in our experiments. The major difference between this study and previous experiments is the role of CO_2. Compared with previous experiments (Berndt et al., 1996; Seyfried et al., 2007; Dufaud et al., 2009; Jones et al., 2010; Marcaillou et al., 2011; Klein and McCollom, 2013; Shibuya et al., 2013), the concentration of CO_2 in this study is significantly higher. During the experiments, the minerals would react with water to liberate Mg^{2+}, Fe^{2+}, and $SiO_{2(aq)}$ to the solution. If the solution is rich in CO_2, the dissolved Mg^{2+} and Fe^{2+} will react with $CO_{2(aq)}$ to form Fe-bearing magnesite. This reaction can be enhanced under high CO_2 partial pressures as achieved in this study. Meanwhile, the concentration of the residual Mg^{2+} and $SiO_{2(aq)}$ is critical in determining the species of the formed silicates. This phenomenon is previously reported by Klein and McCollom (2013), in which they found that serpentinization would cease after the injection of the CO_2-rich fluid to the reaction system and followed by the formation of talc.

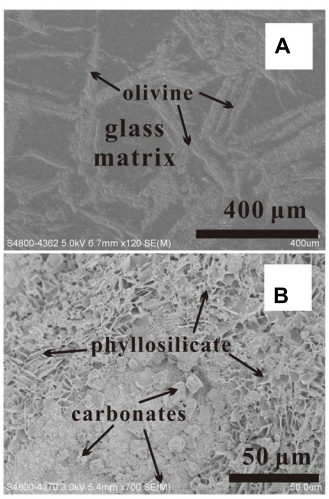

FIGURE 7 | SEM observations showing the surface of komatiite before **(A)** and after **(B)** experiment. The typical secondary minerals are phyllosilicate and carbonate (400°C).

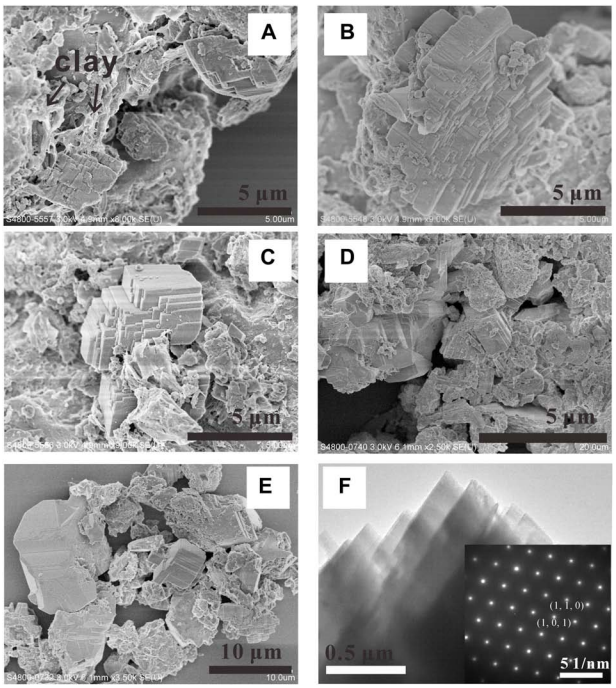

FIGURE 8 | SEM observations **(A–E)** of magnesite formed in the [H_2O-CO_2]-komatiite system. **(F)** TEM image of magnesite crystal and the related SAED pattern.

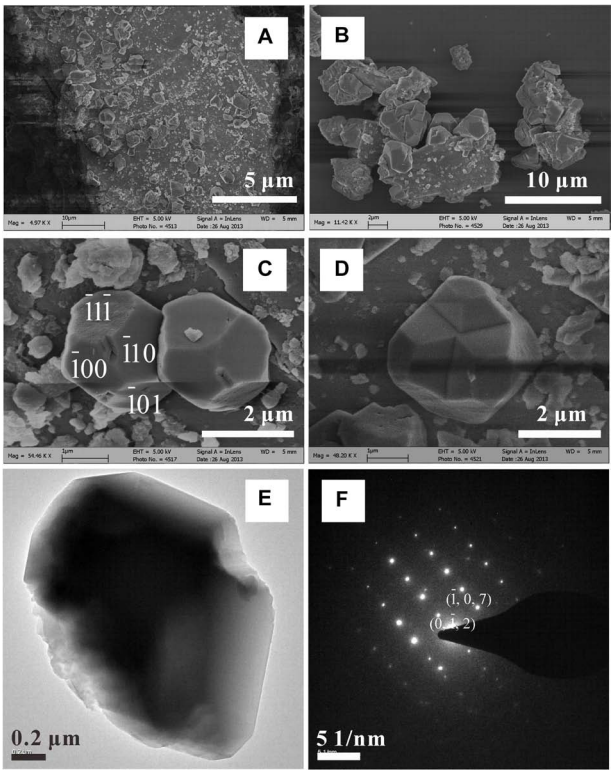

FIGURE 9 | SEM characterizations **(A–D)** of magnesite crystals formed in the [H_2O-CO_2]-peridotite system at 200°C. **(E)** TEM characterization of one single magnesite crystal and the related SAED pattern **(F)**.

Otherwise, serpentine will form under the CO_2-free condition (Berndt et al., 1996; Seyfried et al., 2007; Marcaillou et al., 2011).

Carbonate Speciation

The results indicate that both the reaction temperature and precursor rock type contribute to the speciation of carbonates. Carbonates could not be observed in experiments carried out at temperatures higher than 400°C for all the three reaction systems. Instead of carbonates, fibrous actinolite was formed in komatiite/peridotite systems at higher temperatures. The petrologic difference of the precursor rocks also has an effect on the speciation of carbonate, for example, dolomite is produced in basalt-(H_2O-CO_2) systems while magnesite is formed in the komatiite/peridotite-(H_2O-CO_2) systems at the same reacting temperature (e.g., 200°C).

Because of the high CO_2 partial pressures and relatively small amount of starting rock powder in the gold capsule throughout those experiments, the alkali metal ions extracted by the fluid-rock interaction were insufficient to make the solution alkaline. As a result, the fluid in the Au capsule was probably slightly acidic. Under such considerations, carbonate speciation is controlled by the ionic composition of the fluid in each experiment. As shown in **Figure 12**, the formation of carbonates is constrained by the activities of Ca^{2+}, Mg^{2+}, and dissolved $SiO_{2(aq)}$ in the fluid. Higher temperatures (>400°C) would speed up the alteration and increase the activity of dissolved SiO_2 in the fluid, which gives rise to the formation of actinolite (Fe-containing tremolite) and inhibits the formation of carbonates. When the experimental temperature is lower than 400°C, the reaction becomes slower and the lower activity of dissolved SiO_2 makes the formation of carbonates possible. In this situation, the speciation of carbonate is controlled by the activities of Ca^{2+} and Mg^{2+} in the fluid.

Experimental Conditions That Affect the Production of H_2 and Light Alkanes

GC analyses have shown that H_2 and light alkanes were produced in the batch experiments. Further investigations would be required to ascertain the exact nature of the formation process of these auxiliary compounds, however, we can offer rational explanations. As described in previous studies (Barnes et al., 1972; Moody, 1976; Berndt et al., 1996; Marcaillou et al., 2011), H_2 could be produced during the serpentinization of ultramafic rocks owing to the oxidation of Fe(II) to Fe(III) by water. Control experiments (C-400 and C-500) showed that detectable H_2 could be produced without the addition of ultramafic rocks under higher temperatures (above 400°C), probably due to the oxidation of Ag generated by thermal decomposition of $Ag_2C_2O_4$ (**Supplementary Table S3**).

Light alkanes can form by a variety of chemical pathways. Since H_2 can be produced directly by the water–rock interactions, coupled with the reduction of ferrous iron and probably the formation of magnetite (Hao and Li, 2015), Fischer-Tropsch

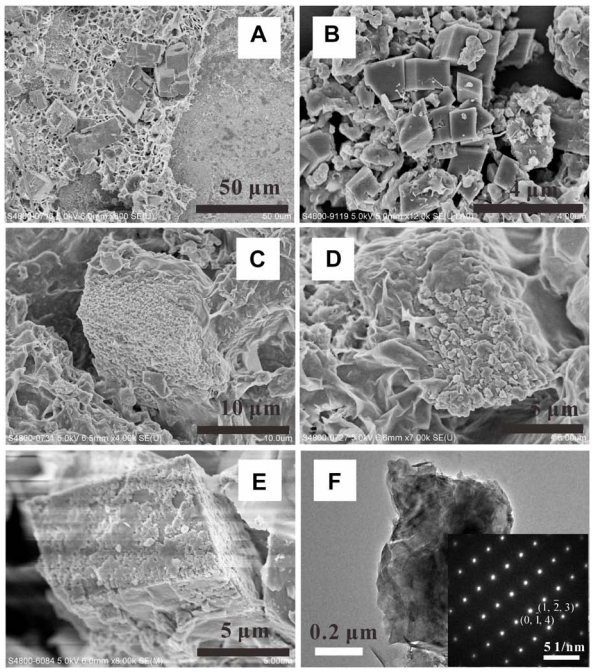

FIGURE 10 | SEM observations of dolomite crystals formed in [H_2O-CO_2]-komatiite system **(A,C)**, [H_2O-CO2]-basalt system **(B)**, and [H_2O-CO_2]-peridotite system **(D,E)**. **(F)** TEM characterization of one dolomite crystal and the related SAED pattern.

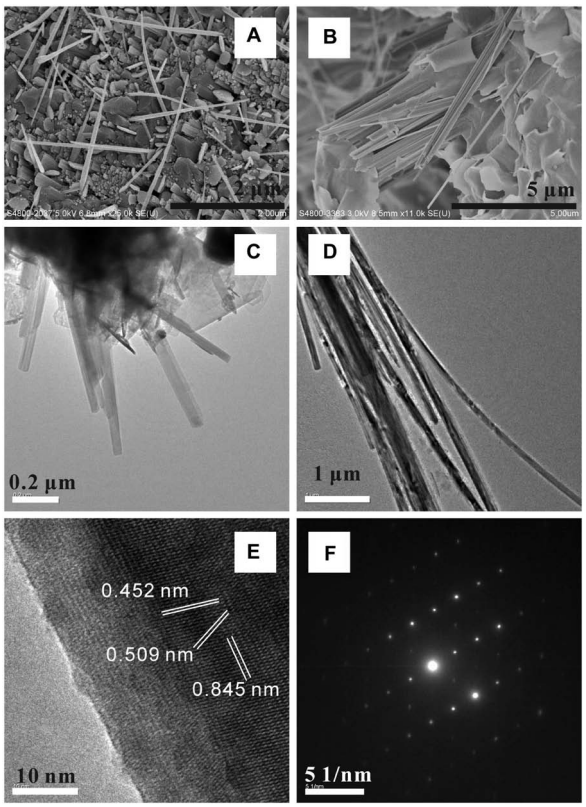

FIGURE 11 | SEM and TEM characterizations of actinolite fiber bundles formed in [H_2O-CO_2]-komatiite system **(A,C)** and [H_2O-CO_2]-peridotite system **(B,D)**. **(E)** HRTEM image of the crystal showing clear lattice fringes. The measured spacings of the crystallographic planes are 0.845, 0.509, and 0.452 nm, respectively. **(F)** SAED pattern of one single actinolite crystal.

synthesis of alkanes might have occurred in our reaction systems with the absence of initial H_2. Previous studies (McCollom and Seewald, 2001; Foustoukos and Seyfried, 2004; Lazar et al., 2012) have shown that light alkanes including CH_4, C_2H_6, and C_3H_8 can be produced in hydrothermal experiments, however, the ^{13}C labeling technique used in those experiments indicated that only a proportion of CH_4 was produced by the reduction of CO_2. Therefore, further experiments performed with ^{13}C-labeled carbon source (e.g., $Ag_2{}^{13}C_2O_4$) need to be conducted to evaluate the possible contribution of background sources to the observed light alkanes.

Compositional Change of the Proto-Atmosphere and Influence on the Earth's Surface Temperature

After the surface heat flow of the Earth was lower than 150 W/m^2, the surface of the Earth rapidly cooled down and the ultramafic proto-crust was formed (Pinti, 2005; Zahnle et al., 2007), which could react with the super-critical H_2O-CO_2 atmosphere immediately, as experimentally demonstrated in this study. Once Earth's surface temperature fell below 400°C, the planetary-wide precipitated carbonates would sequestrate the atmospheric CO_2. Consequently, the rapid removal of CO_2 from the atmosphere would significantly reduce the greenhouse effect and accelerate the cooling of Earth's surface. This cooling facilitated condensation of atmospheric water vapor and the formation of the earliest ocean (Pinti, 2005).

As the carbonates formed by the planetary-wide atmosphere-crust interactions would probably be transported to the mantle in several tens of millions of years (Zahnle et al., 2007), a relatively low CO_2 partial pressure was assumed. The surface temperature of the Earth could fall below the freezing point of water with low CO_2 concentrations because the Sun was approximately 30% less bright when it formed at 4.6 Ga (Schwarzschild, 1958). However, our experiments have shown that CH_4 and H_2 can be effectively produced by atmosphere-crust interactions. They are both candidates of strong greenhouse gasses to keep the Earth's surface warm when the Sun was still young and faint.

Scenario of the Surface Interaction Occurred on the Early Earth and Earth-Like Planets

The Early Earth

Based on the experimental simulation, it is indicated that the interaction between lithological materials and the putative H_2O-CO_2 atmosphere could result in the formation of various clay minerals and carbonates before the formation of the earliest ocean when Earth's surface temperature was higher than 300°C. Because of this planetary-widely

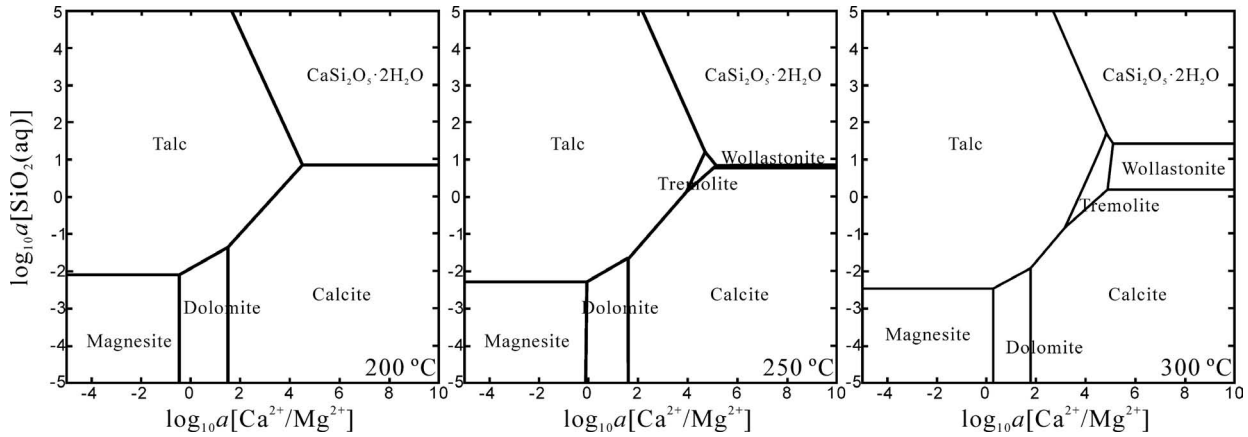

FIGURE 12 | The activity diagrams of the Ca-Mg-Si-H-O-C system at 200–300°C and 50 MPa. The diagrams are calculated with Geochemist's Workbench (Bethke, 1996) using the Lawrence Livermore National Laboratory database. Although the upper limit of temperature is restricted to 300°C, the change of the equilibrium area of tremolite with temperature suggests that it could probably become the most stable phase with relatively higher SiO2(aq) activity and $\log_{10}a[Ca^{2+}]/[Mg^{2+}]$ with higher temperature.

alteration, carbonates and clay minerals may be the major secondary mineral species on Earth's surface in the early Hadean and calcite and dolomite could be the dominant carbonate species. With the cooling of the Earth's surface, magnesite might have eventually become the dominant carbonates species. According to this study, the co-existence of different ultramafic rock, clay and carbonate assemblages may reflect different forming temperatures. Calcite, clay and ultramafic rock assemblages may indicate a relatively higher forming temperature; while magnesite, clay and ultramafic rock assemblages may represent a relatively low temperature alteration.

Clay minerals (smectite and illite) are the most abundant secondary minerals produced by the H_2O-CO_2-rock reactions. These layered clay minerals possess good biocompatibility, strong adsorption, ion exchangeability and expansibility (Ertem, 2004; Zhang et al., 2010; Zhou, 2011; Tran and James, 2012; Zhou and Keeling, 2013). They can absorb various biomolecules including proteins, DNAs and RNAs in the natural environment (Biondi et al., 2007; Cai et al., 2008; Wu et al., 2012). Therefore, they could play an important role in the origin of life and biogeochemical evolution in the early biosphere. When the surface temperature fell below 300°C, the water vapor in the proto-atmosphere would condense to form the earliest oceans (Pinti, 2005). Previously formed clay minerals might pervade the earliest ocean. In this case, reactions associated with the concentration and polymerization of RNA and the production of biopolymers by clay minerals might have happened at an earlier stage. This process may happen several hundred million years before there is geological evidence for early life (Schidlowski, 1988). Meanwhile, the small crystal size of the clay minerals would cause surface reactions to occur at a rather high rate. The biomolecule-clay mineral complexes could protect the biopolymers against strong radiation, bio- or photo-degradation and inactivation (Ferris et al., 1996; Hanczyc et al., 2003; Huang and Ferris, 2003; Saladino et al., 2004) and finally facilitated the origin of life on Earth (Ferris, 2002; Franchi et al., 2003). Since the global occurrence of the reaction between the ultramafic crust and the CO_2-H_2O dominant atmosphere, these processes would probably be widespread instead of being restricted to hydrothermal environments.

Earth-Like Planet – Mars

The putative surface interactions occurring on the other rocky planets may be similar to that has happened to the earliest Earth. Taken Mars as an example, the earliest atmosphere of Mars was theorized to be rich in CO_2 and water similar to Earth's ancient atmosphere (O'Connor, 1968; Booth and Kieffer, 1978; Gooding, 1978; Pollack et al., 1987; Forget and Pierrehumbert, 1997; Catling, 1999; Morse and Marion, 1999; Nakamura and Tajika, 2001; Longhi, 2006; Quinn et al., 2006). Accordingly, the interaction between the atmosphere, the hydrosphere and the lithosphere occurred at the early stage might also lead to the precipitation of clay minerals and carbonates. Recent findings of carbonate by CRISM on MRO (Ehlmann et al., 2008) and the rover Spirit (Morris et al., 2010) provided the strongest lines of evidence for carbonates on Mars in its early evolutionary stage. Currently, igneous rocks interacting with the atmosphere (Farquhar et al., 1998), low temperature aqueous processes (Kirschvink et al., 1997; Valley et al., 1997) and hydrothermal processes (Treiman et al., 2002) have been considered to have contributed to the formation of Martian carbonates. Our experimental results provide an alternative interpretation. Although the atmospheric pressure on early Mars may not have been as high as on the early Earth, we could also expect the occurrence of similar interactions between its H_2O-CO_2 atmosphere and the crust after the planetary accretion. As a result, carbonates and phyllosilicates could have been generated and accumulated on the surface of the planet at the early age. Carbonates and clay minerals produced in this process might

at least constitute part of the ancient rocks on Mars besides the genesis related to aqueous alterations.

CONCLUSION

In this study, batch experiments were performed to investigate the interaction between the proto-atmosphere and the rocky crust on the Hadean Earth and its impact on the subsequent evolution of the surface environment toward a habitable planet. The experimental simulation showed that phyllosilicates and carbonates could probably be produced extensively on the early Hadean Earth. Before the formation of the earliest ocean, the Earth's surface was likely covered by massive carbonates and phyllosilicates, which can also be inferred by the recent discovery of layered clay minerals and carbonate assemblages on Mars. The volatile components in the Au capsule after the batch experiments include hydrogen, CH_4, C_2H_6, and C_3H_8 for most experiments, however, the generation of C_2H_6, C_3H_8, and part of CH_4 may be the result of the decomposition of organic contamination in batch experiments. The H_2 and methane produced by the planetary-wide processes might have been accumulated to a relatively high concentration in the proto-atmosphere. The resulting greenhouse effect may have been strong enough for the early Earth to keep its surface warm against a faint young Sun and guarantee the continuous organochemical evolution toward life.

AUTHOR CONTRIBUTIONS

Y-LL designed the project. X-LH wrote the main manuscript text, prepared the figures, performed the experiments, and all the related analyses. All authors participated in the discussion and commented on the paper.

FUNDING

This study was financially supported by Research Grants Council of Hong Kong (No. 17312016) and the National Natural Science Foundation of China (No. 41506082).

ACKNOWLEDGMENTS

We thank Professor Weidong Sun and Dr. Xing Ding for their advice on our experiments and support from the Hydrothermal Laboratory at Guangzhou Institute of Geochemistry, Chinese Academy of Sciences.

SUPPLEMENTARY MATERIAL

The Supplementary Material for this article can be found online at: https://www.frontiersin.org/articles/10.3389/feart.2018.00180/full#supplementary-material

REFERENCES

Ahrens, T. J., O'Keefe, J. D., and Lange, M. A. (1989). "Formation of atmospheres during accretion of the terrestrial planets," in *Origin and Evolution of Planetary and Satellite Atmospheres*, eds S. K. Atreya, J. B. Pollack, and M. S. Matthews (Tucson, AZ: University of Arizona Press), 328–385.

Barnes, I., Sheppard, R. A., Gude, A. J., Rapp, J. B., and O'Neil, J. R. (1972). Metamorphic assemblages and the direction of flow of metamorphic fluids in 4 instances of serpentinization. *Contrib. Mineral. Petrol.* 35, 263–276. doi: 10.1007/BF00371220

Berndt, M. E., Allen, D. E., and Seyfried, W. E. (1996). Reduction of CO_2 during serpentinization of olivine at 300°C and 500 bar. *Geology* 24, 351–354. doi: 10.1130/0091-7613(1996)024<0351:ROCDSO>2.3.CO;2

Berry, A. J., Danyushevsky, L. V., O'Neill, H. S. C., Newville, M., and Sutton, S. R. (2008). Oxidation state of iron in komatiitic melt inclusions indicates hot Archaean mantle. *Nature* 455, 960–963. doi: 10.1038/nature07377

Bethke, C. M. (1996). *Geochemical Reaction Modeling: Concepts and Applications*. New York, NY: Oxford University Press.

Biondi, E., Branciamore, S., Fusi, L., Gago, S., and Gallori, E. (2007). Catalytic activity of hammerhead ribozymes in a clay mineral environment: implications for the RNA world. *Gene* 389, 10–18. doi: 10.1016/j.gene.2006.09.002

Booth, M. C., and Kieffer, H. H. (1978). Carbonate formation in Mars-like environments. *J. Geophys. Res.* 83, 1809–1815. doi: 10.1029/JB083iB04p01809

Cai, P., Huang, Q. Y., Li, M., and Liang, W. (2008). Binding and degradation of DNA on montmorillonite coated by hydroxyl aluminum species. *Colloids Surf. B Biointerfaces* 62, 299–306. doi: 10.1016/j.colsurfb.2007.10.016

Canil, D. (1997). Vanadium partitioning and the oxidation state of komatiite magmas. *Nature* 389, 842–845. doi: 10.1038/39860

Catling, D. C. (1999). A chemical model for evaporites on early Mars: possible sedimentary tracers of the early climate and implications for exploration. *J. Geophys. Res. Planets* 104, 16453–16469. doi: 10.1029/1998JE001020

Condie, K. C. (1980). Origin and early development of the Earth's Crust. *Precambrian Res.* 11, 183–197. doi: 10.1016/0301-9268(80)90064-9

Delano, J. W. (2001). Redox history of the Earth's interior since 3900 Ma: implications for prebiotic molecules. *Orig. Life Evol. Biosph.* 31, 311–341. doi: 10.1023/A:1011895600380

Dufaud, F., Martinez, I., and Shilobreeva, S. (2009). Experimental study of Mg-rich silicates carbonation at 400 and 500 °C and 1 kbar. *Chem. Geol.* 262, 344–352. doi: 10.1016/j.chemgeo.2009.01.026

Ehlmann, B. L., Mustard, J. F., Murchie, S. L., Poulet, F., Bishop, J. L., Brown, A. J., et al. (2008). Orbital identification of carbonate-bearing rocks on Mars. *Science* 322, 1828–1832. doi: 10.1126/science.1164759

Ertem, G. (2004). Montmorillonite, oligonucleotides, RNA and origin of life. *Orig. Life Evol. Biosph.* 34, 549–570. doi: 10.1023/B:ORIG.0000043130.49790.a7

Farquhar, J., Thiemens, M. H., and Jackson, T. (1998). Atmosphere-surface interactions on Mars: delta O-17 measurements of carbonate from ALH 84001. *Science* 280, 1580–1582. doi: 10.1126/science.280.5369.1580

Ferris, J. P. (2002). Montmorillonite catalysis of 30-50 mer oligonucleotides: laboratory demonstration of potential steps in the origin of the RNA world. *Orig. Life Evol. Biosph.* 32, 311–332. doi: 10.1023/A:1020543312109

Ferris, J. P., Hill, A. R., Liu, R. H., and Orgel, L. E. (1996). Synthesis of long prebiotic oligomers on mineral surfaces. *Nature* 381, 59–61. doi: 10.1038/381059a0

Forget, F., and Pierrehumbert, R. T. (1997). Warming early Mars with carbon dioxide clouds that scatter infrared radiation. *Science* 278, 1273–1276. doi: 10.1126/science.278.5341.1273

Foustoukos, D. I., and Seyfried, W. E. (2004). Hydrocarbons in hydrothermal vent fluids: the role of chromium-bearing catalysts. *Science* 304, 1002–1005. doi: 10.1126/science.1096033

Franchi, M., Ferris, J. P., and Gallori, E. (2003). Cations as mediators of the adsorption of nucleic acids on clay surfaces in prebiotic environments. *Orig. Life Evol. Biosph.* 33, 1–16. doi: 10.1023/A:1023982008714

Gooding, J. L. (1978). Chemical weathering on Mars - Thermodynamic stabilities of primary minerals (and their alteration products) from mafic igneous rocks. *Icarus* 33, 483–513. doi: 10.1016/0019-1035(78)90186-0

Hanczyc, M. M., Fujikawa, S. M., and Szostak, J. W. (2003). Experimental models of primitive cellular compartments: encapsulation, growth, and division. *Science* 302, 618–622. doi: 10.1126/science.1089904

Hao, X. L., and Li, Y. L. (2013). Fe-57 Mössbauer spectroscopy of mineral assemblages in mantle spinel lherzolites from Cenozoic alkali basalt, eastern China: petrological applications. *Lithos* 156, 112–119. doi: 10.1016/j.lithos.2012.10.016

Hao, X. L., and Li, Y. L. (2015). Hexagonal plate-like magnetite nanocrystals produced in komatiite-H_2O-CO_2 reaction system at 450°C. *Int. J. Astrobiol.* 14, 547–553. doi: 10.1017/S1473550415000014

Hazen, R. M., Downs, R. T., Kah, L., and Sverjensky, D. (2013). Carbon mineral evolution. *Carbon Earth* 75, 79–107. doi: 10.2138/rmg.2013.75.4

Hazen, R. M., Papineau, D., Leeker, W. B., Downs, R. T., Ferry, J. M., McCoy, T. J., et al. (2008). Mineral evolution. *Am. Mineral.* 93, 1693–1720. doi: 10.2138/am.2008.2955

Holland, H. D. (1984). *The Chemical Evolution of the Atmosphere and Oceans*. Princeton, NJ: Princeton University Press, 582.

Huang, W. H., and Ferris, J. P. (2003). Synthesis of 35-40 mers of RNA oligomers from unblocked monomers. A simple approach to the RNA world. *Chem. Commun.* 9, 1458–1459. doi: 10.1039/B303134A

Jones, L. C., Rosenbauer, R., Goldsmith, J. I., and Oze, C. (2010). Carbonate control of H_2 and CH_4 production in serpentinization systems at elevated P-Ts. *Geophys. Res. Lett.* 37:L14306. doi: 10.1029/2010GL043769

Kasting, J. F. (1993). Earth's early atmosphere. *Science* 259, 920–926. doi: 10.1126/science.11536547

Kirschvink, J. L., Maine, A. T., and Vali, H. (1997). Paleomagnetic evidence of a low-temperature origin of carbonate in the Martian meteorite ALH84001. *Science* 275, 1629–1633. doi: 10.1126/science.275.5306.1629

Klein, F., and McCollom, T. M. (2013). From serpentinization to carbonation: new insights from a CO_2 injection experiment. *Earth Planet. Sci. Lett.* 379, 137–145. doi: 10.1016/j.epsl.2013.08.017

Lange, M. A., and Ahrens, T. J. (1982). The evolution of an impact-generated atmosphere. *Icarus* 51, 96–120. doi: 10.1016/0019-1035(82)90031-8

Lazar, C., McCollom, T. M., and Manning, C. E. (2012). Abiogenic methanogenesis during experimental komatiite serpentinization: implications for the evolution of the early Precambrian atmosphere. *Chem. Geol.* 326–327, 102–112. doi: 10.1016/j.chemgeo.2012.07.019

Li, Z. X. A., and Lee, C. T. (2004). The constancy of upper mantle fO_2 through time inferred from V/Sc ratios in basalts. *Earth Planet. Sci. Lett.* 228, 483–493. doi: 10.1016/j.epsl.2004.10.006

Liu, L. G. (2004). The inception of the oceans and CO_2-atmosphere in the early history of the Earth. *Earth Planet. Sci. Lett.* 227, 179–184. doi: 10.1016/j.epsl.2004.09.006

Longhi, J. (2006). Phase equilibrium in the system CO_2-H_2O: application to Mars. *J. Geophys. Res. Planets* 111:E06011. doi: 10.1029/2005JE002552

Marcaillou, C., Munoz, M., Vidal, O., Parra, T., and Harfouche, M. (2011). Mineralogical evidence for H_2 degassing during serpentinization at 300 degrees C/300 bar. *Earth Planet. Sci. Lett.* 303, 281–290. doi: 10.1016/j.epsl.2011.01.006

Martin, H., Albarede, F., Claeys, P., Gargaud, M., Marty, B., Morbidelli, A., et al. (2006). Building of a habitable planet. *Earth Moon Planets* 98, 97–151. doi: 10.1007/s11038-006-9088-4

McCollom, T. M., and Seewald, J. S. (2001). A reassessment of the potential for reduction of dissolved CO_2 to hydrocarbons during serpentinization of olivine. *Geochim. Cosmochim. Acta* 65, 3769–3778. doi: 10.1016/S0016-7037(01)00655-X

Moody, J. B. (1976). Serpentinization: a review. *Lithos* 9, 125–138. doi: 10.1016/0024-4937(76)90030-X

Morris, R. V., Ruff, S. W., Gellert, R., Ming, D. W., Arvidson, R. E., Clark, B. C., et al. (2010). Identification of carbonate-rich outcrops on Mars by the Spirit Rover. *Science* 329, 421–424. doi: 10.1126/science.1189667

Morse, J. W., and Marion, G. M. (1999). The role of carbonates in the evolution of early martian oceans. *Am. J. Sci.* 299, 738–761. doi: 10.2475/ajs.299.7-9.738

Nakamura, T., and Tajika, E. (2001). Stability and evolution of the climate system of Mars. *Earth Planets Space* 53, 851–859. doi: 10.1186/BF03351682

Nisbet, E. G., Arndt, N. T., Bickle, M. J., Cameron, W. E., Chauvel, C., Cheadle, M., et al. (1987). Uniquely fresh 2.7 Ga komatiites from the belingwe greenstone-belt. *Zimb. Geol.* 15, 1147–1150. doi: 10.1130/0091-7613(1987)15<1147:UFGKFT>2.0.CO;2

O'Connor, J. T. (1968). Mineral stability at the Martian surface. *J. Geophys. Res.* 73, 5301–5311. doi: 10.1029/JB073i016p05301

Pearce, J. A. (1976). Statistical analysis of major element patterns in basalts. *J. Petrol.* 17, 15–43. doi: 10.1093/petrology/17.1.15

Pinti, D. L. (2005). "The origin and evolution of the oceans," in *Lectures in Astrobiology*, Vol. 1, eds B. Barbier, H. Martin, and J. Reisse (Berlin: Springer), 83–112.

Pollack, J. B., Kasting, J. F., Richardson, S. M., and Poliakoff, K. (1987). The case for a wet, warm climate on early Mars. *Icarus* 71, 203–224. doi: 10.1016/0019-1035(87)90147-3

Quinn, R., Zent, A. P., and McKay, C. P. (2006). The photochemical stability of carbonates on Mars. *Astrobiology* 6, 581–591. doi: 10.1089/ast.2006.6.581

Saladino, R., Crestini, C., Ciambecchini, U., Ciciriello, F., Costanzo, G., and Di Mauro, E. (2004). Synthesis and degradation of nucleobases and nucleic acids by formamide in the presence of montmorillonites. *Chembiochem* 5, 1558–1566. doi: 10.1002/cbic.200400119

Schidlowski, M. (1988). A 3,800 million-year old record of life from carbon in sedimentary rocks. *Nature* 333, 313–318. doi: 10.1038/333313a0

Schwarzschild, M. (1958). *Structure and Evolution of the Stars*. Princeton, NJ: Princeton University Press. doi: 10.1515/9781400879175

Seyfried, W. E., Foustoukos, D. I., and Fu, Q. (2007). Redox evolution and mass transfer during serpentinization: an experimental and theoretical study at 200 degrees C, 500 bar with implications for ultramafic-hosted hydrothermal systems at Mid-Ocean Ridges. *Geochim. Cosmochim. Acta* 71, 3872–3886. doi: 10.1016/j.gca.2007.05.015

Shaw, G. H. (2008). Earth's atmosphere - Hadean to early Proterozoic. *Chem. Erde* 68, 235–264. doi: 10.1016/j.chemer.2008.05.001

Shibuya, T., Yoshizaki, M., Masaki, Y., Suzuki, K., Takai, K., and Russell, M. J. (2013). Reactions between basalt and CO_2-rich seawater at 250 and 350 degrees C, 500 bars: implications for the CO_2 sequestration into the modern oceanic crust and the composition of hydrothermal vent fluid in the CO_2-rich early ocean. *Chem. Geol.* 359, 1–9. doi: 10.1016/j.chemgeo.2013.08.044

Sleep, N. H. (2010). The Hadean-Archaean environment. *Cold Spring Harb. Perspect. Biol.* 2:a002527. doi: 10.1101/cshperspect.a002527

Sleep, N. H., and Zahnle, K. (2001). Carbon dioxide cycling and implications for climate on ancient Earth. *J. Geophys. Res. Planets* 106, 1373–1399. doi: 10.1029/2000JE001247

Tessalina, S. G., Bourdon, B., Van Kranendonk, M., Birck, J. L., and Philippot, P. (2010). Influence of Hadean crust evident in basalts and cherts from the Pilbara Craton. *Nat. Geosci.* 3, 214–217. doi: 10.1038/ngeo772

Trail, D., Watson, E. B., and Tailby, N. D. (2011). The oxidation state of Hadean magmas and implications for early Earth's atmosphere. *Nature* 480, 79–82. doi: 10.1038/nature10655

Tran, A. T. T., and James, B. J. (2012). A study the interaction forces between the bovine serum albumin protein and montmorillonite surface. *Colloids Surf. A Physicochem. Eng. Asp.* 414, 104–114. doi: 10.1016/j.colsurfa.2012.08.066

Treiman, A. H., Amundsen, H. E. F., Blake, D. F., and Bunch, T. (2002). Hydrothermal origin for carbonate globules in Martian meteorite ALH84001: a terrestrial analogue from Spitsbergen (Norway). *Earth Planet. Sci. Lett.* 204, 323–332. doi: 10.1016/S0012-821X(02)00998-6

Valley, J. W., Cavosie, A. J., Ushikubo, T., Reinhard, D. A., Lawrence, D. F., Larson, D. J., et al. (2014). Hadean age for a post-magma-ocean zircon confirmed by atom-probe tomography. *Nat. Geosci.* 7, 219–223. doi: 10.1038/ngeo2075

Valley, J. W., Eiler, J. M., Graham, C. M., Gibson, E. K., Romanek, C. S., and Stolper, E. M. (1997). Low-temperature carbonate concretions in the Martian meteorite ALH84001: evidence from stable isotopes and mineralogy. *Science* 275, 1633–1638. doi: 10.1126/science.275.5306.1633

Walker, J. C. G. (1985). Carbon-dioxide on the early Earth. *Orig. Life Evol. Biosph.* 16, 117–127. doi: 10.1007/BF01809466

Wilde, S. A., Valley, J. W., Peck, W. H., and Graham, C. M. (2001). Evidence from detrital zircons for the existence of continental crust and oceans on the Earth 4.4 Gyr ago. *Nature* 409, 175–178. doi: 10.1038/35051550

Wu, L. M., Zhou, C. H., Keeling, J., Tong, D. S., and Yu, W. H. (2012). Towards an understanding of the role of clay minerals in crude oil formation, migration

and accumulation. *Earth Sci. Rev.* 115, 373–386. doi: 10.1016/j.earscirev.2012.10.001

Yu, H. M., Xia, Q. K., Dallai, L., and Chazot, G. (2005a). Oxygen isotope and trace element compositions of peridotite xenoliths from Nushan volcano, SE China and implications for mantle metasomatism. *Acta Petrol. Sin.* 21, 829–838.

Yu, H. M., Xia, Q. K., Wang, R. C., and Chen, X. M. (2005b). Oxygen isotope and trace element compositions of peridotite xenoliths from Panshishan volcano, SE China. *Acta Petrol. Sin.* 21, 1609–1616.

Zahnle, K., Arndt, N., Cockell, C. S., Halliday, A., Nisbet, E., Selsis, F., et al. (2007). Emergence of a habitable planet. *Space Sci. Rev.* 129, 35–78. doi: 10.1007/s11214-007-9225-z

Zahnle, K. J. (2006). Earth's earliest atmosphere. *Elements* 2, 217–222. doi: 10.2113/gselements.2.4.217

Zhang, D., Zhou, C. H., Lin, C. X., Tong, D. S., and Yu, W. H. (2010). Synthesis of clay minerals. *Appl. Clay Sci.* 50, 1–11. doi: 10.1016/j.clay.2010.06.019

Zhou, C. H. (2011). An overview on strategies towards clay-based designer catalysts for green and sustainable catalysis. *Appl. Clay Sci.* 53, 87–96. doi: 10.1016/j.clay.2011.04.016

Zhou, C. H., and Keeling, J. (2013). Fundamental and applied research on clay minerals: from climate and environment to nanotechnology. *Appl. Clay Sci.* 74, 3–9. doi: 10.1016/j.clay.2013.02.013

Conflict of Interest Statement: The authors declare that the research was conducted in the absence of any commercial or financial relationships that could be construed as a potential conflict of interest.